R-10-24

System and safety studies of accelerator driven systems and generation IV reactors for transmutation of minor actinides

Annual report 2009

Calle Berglöf, Andrei Fokau, Mikael Jolkkonen,
Milan Tesinsky, Janne Wallenius, Youpeng Zhang

Division of Reactor Physics, Royal Institute
of Technology, Stockholm

March 2010

Svensk Kärnbränslehantering AB
Swedish Nuclear Fuel
and Waste Management Co

Box 250, SE-101 24 Stockholm
Phone +46 8 459 84 00

ISSN 1402-3091
SKB Rapport R-10-24

System and safety studies of accelerator driven systems and generation IV reactors for transmutation of minor actinides

Annual report 2009

Calle Berglöf, Andrei Fokau, Mikael Jolkkonen,
Milan Tesinsky, Janne Wallenius, Youpeng Zhang

Division of Reactor Physics, Royal Institute
of Technology, Stockholm

March 2010

Summary

During 2009, the reactor physics division at KTH has made a design study of a source efficient ADS with nitride fuel and 15/15Ti cladding, based on the EFIT design made within the EUROTRANS project. It was shown that the source efficiency may be doubled as compared to the reference design with oxide fuel and T91 cladding.

Transient analysis of a medium sized sodium cooled reactor with MOX fuel allowed to define criteria in terms of power penalty for americium introduction. It was shown that for each percent of americium added to the fuel, the linear rating must be reduced by 6% in order for the fuel to survive postulated unprotected transients.

The Sjöstrand area ratio method for reactivity determination has been evaluated experimentally in the strongly heterogeneous subcritical facility YALINA-Booster. Surprisingly, it has been found that the area ratio reactivity estimates may differ by a factor of two depending on detector position. It is shown that this strong spatial dependence can be explained based on a two-region point kinetics model and rectified by means of correction factors obtained through Monte Carlo simulations.

For the purpose of measuring high energy neutron cross sections at the SCANDAL facility in Uppsala, Monte Carlo simulations of neutron to proton conversion efficiencies in CsI detectors have been performed.

A uranium fuel fabrication laboratory has been taken into operation at KTH in 2009. Uranium and zirconium nitride powders have been fabricated by hydridation/nitridation of metallic source materials. Sample pellets have been pressed and ZrN discs have been sintered to 93% density by means of spark plasma sintering methods.

Sammanfattning

Under 2009 har avdelningen för reaktorfysik på KTH utformat en källeffektiv ADS med nitrid-bränsle och 15/15Ti-kapsling, baserad på den EFIT-design som tagits fram i EUROTRANS-projektet. Källeffektiviteten i denna ADS är dubbelt så stor som den hos referenssystemet med oxidbränsle och T91-kapsling.

En transientanalys utförd på en modell av en natriumkyld reaktor med MOX-bränsle gjorde det möjligt att definiera effektbegränsningar resulterande från introduktion av americium i bränslet. För varje procent americium som blandas in i bränslet behöver linjäreffekten reduceras med 6% för att bränslet skall klara transienter utan styrstavsinsättning.

Sjöstrands metod för bestämning av reaktivitet har utvärderats experimentellt i det kraftigt heterogena underkritiska systemet YALINA-booster. En oväntat stor skillnad mellan reaktivitetsuppskattningar gjorda med detektorer i olika delar av härden kunde förklaras med en punktkinetisk modell uppdelad i två regioner. Reaktivitetsvärdet kunde sedan korrigeras med hjälp av Monte Carlo-beräkningar.

I syfte att mäta neutrontvärsnitt vid höga energier vid SCANDAL-anläggningen i Uppsala, har Monte Carlo-simuleringar av konverteringseffektivitet från neutroner till protoner i CsI-detektorer utförts.

Ett laboratorium för att tillverka uranbränslen har tagits i drift på KTH under 2009. Uran- och zirkoniumnitridpulver har tillverkats från metalliska material medelst en hydriderings/nitriderings-process. Provkutsar har pressats och ZrN-skivor har kunnat sintras till 93% täthet med hjälp av starkströmassisterad varmpressning.

Contents

1 Introduction

Research on accelerator driven systems (ADS) and Generation IV reactors (Gen-IV) for transmutation of nuclear waste is performed at the division of reactor physics at KTH. In 2009, the major context of this research was the EUROTRANS project in the 6th framework programme of the European Commission, where design of an experimental ADS with MOX fuel and lead-bismuth coolant (XT-ADS) and an industrial demonstration facility for minor actinide transmutation (EFIT) is made. Development of ADS fuel and structural materials are integrated into the project.

The division of reactor physics at KTH is participating in all domains of the EUROTRANS project, in particular with the following activities:

Domain DESIGN:	Co-ordination of the safety work package. Assessment of the source term in case of severe accidents.
Domain ECATS:	Development and testing of methods for sub-criticality monitoring.
Domain AFTRA:	Fuel modelling, Transient safety analysis.
Domain DEMETRA:	Modelling of radiation damage in Fe-Cr-C steels.

Furthermore, KTH participated in the ELSY, PUMA, GETMAT and FAIRFUELS projects, where development of fast neutron lead cooled reactors (ELSY), high temperature gas cooled reactors (PUMA) structural materials for Gen-IV and ADS systems (GETMAT) and fuels for ADS and Gen-IV reactors (FAIRFUELS) are developed, all in the general context of minor actinide transmutation.

In the present report, a summary of activities performed at KTH during 2009 is provided, including an account for participation in conferences and project meetings.

2 ADS design

During 2009, external source efficiency of three fuel options for the European Facility for Industrial Transmutation (EFIT) has been studied based on the reference EFIT core design developed within the Integrated Project EUROTRANS. It was found that the neutron economy of fuel, influencing the EFIT core size, has strong impact on the external source efficiency. Thus, the nitride fuel with ZrN base, featuring excellent neutron economy, allows designing more compact core than that with composite oxide fuels based on MgO and Mo matrix. This significantly boosts the external source efficiency and reduces the coolant void worth. Additionally, adoption of the austenitic steel 15/15Ti as clad material and lead-bismuth eutectic as coolant allows to reduce the fuel pin pitch and therefore the coolant volume fraction in the core, making the neutron energy spectrum faster and consequently increasing minor actinides fission probabilities.

Taking into account neutronic, chemical and safety factors, two composite oxide fuel options have been earlier selected within the FUTURE project /Pillon and Wallenius 2006, Pillon et al. 2003/ of the 5th Framework Programme (FP) of EURATOM. Both fuels are actinide sesquioxide (Pu,Np,Am,Cm) O_{2-x} dispersed in a matrix material, which is MgO for ceramic-ceramic (CERCER) fuel and Mo for ceramic-metallic (CERMET) fuel. Properties of these composite oxide fuels have been investigated in details within the EUROTRANS project /Maschek et al. 2008a/, in which the MgO-based fuel has been selected for the reference design of the EFIT /Artioli et al. 2008/. On the other hand, nitride fuel, featuring good neutron economy and good thermal conductivity /Wallenius et al. 2006/, was considered a back-up option within the EUROTRANS project, due to the lack of experience in fabricating americium-containing nitride fuels.

Recent success in fabrication of (Np,Pu,Am,Cm)N compounds /Arai et al. 2008, Minato et al. 2009/ and good results of (Pu,Zr)N irradiation /Arai et al. 2006, Golovanov et al. 2006, Hilton et al. 2006/ motivate considering nitride fuels for early implementation of ADS technology. A design of 800 MW_{th} ADS with nitride fuel has been earlier proposed /Tsujimoto et al. 2004/ and further optimized /Saito et al. 2006, Nishihara et al. 2008/ by JAEA. The optimized core driven by 1.5 GeV proton source (10.5–15.6 mA) features an energy gain of 35–50 and demonstrates high external source efficiency.

During 2009, neutronic and burnup calculations have been performed in order to compare the EFIT core performance with CERCER, CERMET and nitride fuel. The nitride core has been designed to reach high source efficiency, while the composition of CERMET and nitride fuels has been optimized for reducing the reactivity swing.

2.1 EFIT core models

Table 2.1 gives parameters of models used for neutronic and burnup simulation. The reference design and fuel composition of the EFIT-MgO/Pb core /Artioli et al. 2008/ were used for the CERCER core model. The dimensions of fuel assemblies and fuel pins of the CERMET /Maschek et al. 2008b, Sobolev et al. 2007/ and nitride /Fokau et al. 2010/ cores correspond to the outer zone of EFIT-MgO/Pb, however, the fuel pin pitch in the CERCER core is set to 13.54 mm, and the fuel pin pitch in the nitride core is decreased to 12 mm in order to allow placing of 216 fuel pins. The three-zone loading schemes are presented in Figure 2-1. The good neutron economy of the nitride fuel and the dense fuel pin packing allow lower mass of fissionable material in the nitride core and smaller number of fuel assemblies (78 FA) compared to the reference core (180 FA). In contrary, the worse neutron economy of the CERMET fuel (due to the neutron absorption by molybdenum) requires more fuel assemblies (216 FA), since the matrix fraction must be above 50 vol.% to ensure continuous matrix phase and therefore a good thermal conductivity.

Table 2-1. Parameters of EFIT models used for simulation.

Model parameter	CERCER	CERMET	Nitride
Core power, MW_{th}	384	488	201
k_{eff} at BOL	0.97	0.97	0.97
Proton energy, GeV	0.8	0.8	0.8
Cycle length, EFPD	1,095	1,095	1,095
Average specific power, MW/t_{HM}	71.5	71.5	71.5
Average linear power rating, kW/m	14.1	15.0	13.3
Fuel mass, ton_{HM}	5.4	6.8	2.8
Fuel assemblies	180	216	78
Target area, SA	19	19	7
Target radius, cm	39	39	22
FA pitch, mm	191	191	191
Fuel pins per FA	168	168	216
Active height, m	0.9	0.9	0.9
Fuel pin pitch, mm	13.63/13.54 [a]	13.54	12.0
Fuel pin diameter, mm	8.62/9.52 [a]	9.52	9.52
Pin pitch to diameter ratio	1.58/1.42 [a]	1.42	1.26
Cladding thickness, mm	0.6	0.6	0.6
Gas gap, mm	0.16	0.16	0.16
Fuel form	AnO_{2-x}	AnO_{2-x}	AnN
Matrix/diluent	MgO	Mo [b]	ZrN
Average matrix fraction, vol.%	51.5	54.8	71.8
Pu/(Pu+MA) ratio, at%	45.9	42.0	43.5
Cladding material	T91	T91	15/15Ti
Coolant and target material	Pb	Pb	LBE
Coolant inlet temperature, K	673	651	583
Coolant outlet temperature, K	753	753	753
Coolant temperature increase, K	80	102	170

a) When two values are specified, the first value is for the inner and middle zones, and the second value is for the outer zone.
b) Enriched molybdenum vector.

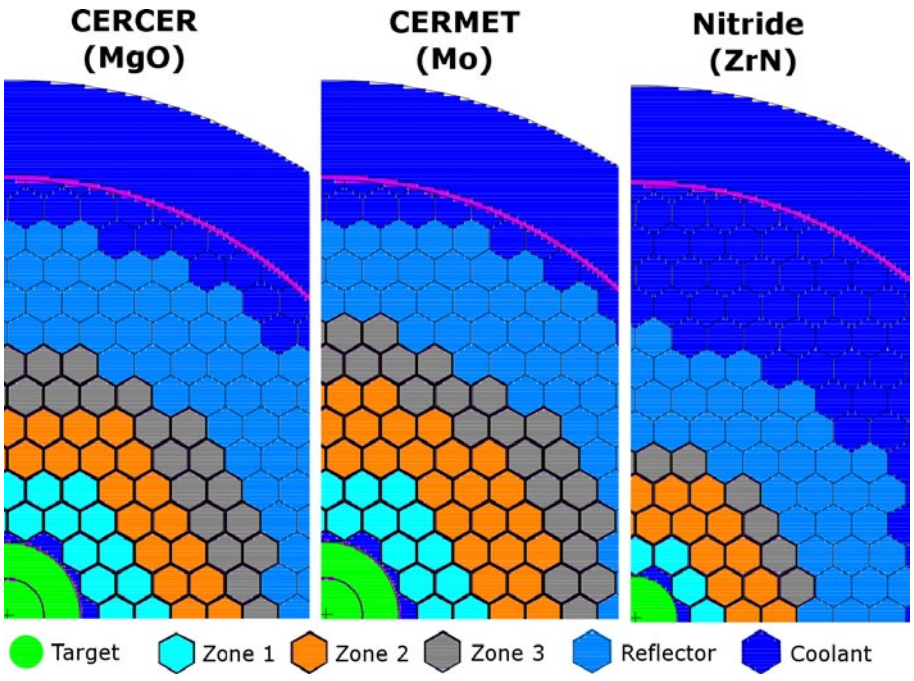

Figure 2-1. *Loading scheme of CERCER (180 FA), CERMET (216 FA) and nitride (78 FA) cores.*

The composition of actinide vectors is given in Table 2-2, together with assumed vector for enriched molybdenum used for CERMET fuel. The nitrogen in the nitride fuel is assumed to be 100% enriched in N-15. The ratio between fuel and matrix (or diluent material) was obtained for each zone in order to minimize radial power peaking factor and to achieve subcriticality of the reference core ($k_{eff} = 0.97$).

Since Ti-modified austenitic steels have a considerably higher creep rupture strength than ferritic-martensitic steels /Cannon et al. 1992/, allowing clad temperatures of up to 1,200 K during transients, adoption of the austenitic steel 15/15Ti as clad material allows us to safely reduce the fuel pin pitch from 1.36 cm (in average) to 1.20 cm. It makes it possible to fit one extra fuel pin row in the fuel assembly geometry, so that the number of fuel pins per assembly is increased from 168 to 216. Safety performance of the new core design was confirmed by a full set of transient analysis /Zhang et al. 2010/.

2.2 Modelling tools

A number of simulations were performed in order to obtain neutronic and burn-up characteristics of the models. An irradiation period of 3 years was used, which corresponds to the maximum allowable radiation damage of the most exposed fuel pin (150 dpa) /Henry 2009/. The Monte Carlo codes MCNPX2.7a /Pelowitz et al. 2008/ and MCB2 /Cetnar et al. 1998/ and the JEFF3.1.1 data library /Koning and Forrest 2006/ were used in the simulations. Neither Doppler broadening, nor gamma heating treatment was applied for the cross-section library. Doppler feedback has previously been shown to be negligible for fuels with americium concentrations exceeding 30%.

A neutron source created by 800 MeV protons has been prepared by means of MCNPX with the LA150 data library /Chadwick et al. 2001/ invoking the CEM03 model /Mashnik et al. 2006/. According to standard procedure, all neutrons leaking to the core from the spallation target (i.e. the source neutrons) were recorded to a surface-source file. MCB code was then applied for both burnup and neutron transport calculations, using only neutrons with energy below 20 MeV from the source file.

In order to estimate the effect of the discarded high energy neutrons at the Beginning-Of-Life (BOL), we have compared the number of fissions per proton calculated by the two step approach with MCB, to those obtained by the direct calculation by MCNPX. As shown in Table 2-3, the source efficiency of the nitride core is 20.5% higher when the high energy neutrons are considered. In order to take this effect into account, the correction factors listed in Table 2-4 have been applied to affected parameters, such as neutron source efficiency, φ^* /Salvatores et al. 1997/, and proton source efficiency, ψ^* /Seltborg et al. 2003/.

Table 2-2. Actinide vectors used for core simulation /Sobolev 2007/ and assumed molybdenum vector.

Pu	**238**	**239**	**240**	**241**	**242**	**244**	
at.%	3.7	46.4	34.1	3.8	11.9	1.2E–3	
Cm	**243**	**244**	**245**	**246**	**247**	**248**	
at.%	1.5	69.8	26.5	2.1	4.0E–2	2.3E–3	
Am	**241**	**242m**	**243**	**MA**	**Np**	**Am**	**Cm**
at.%	82.2	0.3	17.5	at.%	3.9	91.8	4.3
Mo	**92**	**94**	**95**	**96**			
at.%	92.9	6.1	1.0	0.1			

Table 2-3. Impact of high energy source neutrons on source efficiency at BOL.

Core model	Target radius, cm	Fraction of source neutrons above 20 MeV, %	Number of fissions per source proton	
			MCNPX and MCB	MCNPX only
Nitride	22	2.8	165	199 (+20.5%)
CERCER	39	1.5	112	128 (+14.1%)
CERMET	39	1.5	91	98 (+8.1%)

Table 2-4. Correction factors used to take into account effect of high energy source neutrons.

Correction for	Nitride	CERCER	CERMET
Proton source efficiency	1.205	1.141	1.081
Source neutrons per proton	1.028	1.015	1.015
Neutron source efficiency	1.173	1.125	1.065

2.3 Results of modelling and optimization

As shown in Table 2-5, the smaller core size and smaller target area of the nitride core result in a 80% higher proton source efficiency, while the CERMET core is 18% less source efficient than the CERCER core. The smaller core power and higher source efficiency lower the demand on proton current by 67%. Using the definition of source neutrons given above and applying the correction factors discussed earlier, the neutron source efficiency for the nitride core becomes 0.95, or 76% higher than that of the CERCER core. As a result of the smaller target, the source neutrons energy is higher for the nitride core providing higher fission probabilities and higher number of secondary neutrons produced by (n,xn) reactions /Seltborg and Jacqmin 2001, Yang et al. 2001/. Finally, our calculations show that the energy gain of the nitride core is 53, assuming average fission energy release of 215 MeV per fission, including capture and decay heat. Note, that due to the reactivity swing of the composite oxide cores, the values of their energy gain tend to get worse during fuel burnup. It should be noted, that the proton source efficiency of the EFIT cores may also be reduced for the equilibrium cycle, and therefore needs to be studied.

The reactivity swing (change of the reactivity during fuel burnup) was studied by analysing swings of the effective multiplication factor without source, k_{eff}, and the effective multiplication factor with source, k_s /Dulla et al. 2006/. A significant difference between the swing of k_{eff}, and the swing of k_s is obtained for the composite oxide fuels (see Table 2-6 and Figure 2-2). However, this difference is negligible for the nitride fuel due to the neutron source efficiency being close to unity. Moreover, both k_{eff} and k_s of the nitride core have very low swings during 3 years of operation from the BOL.

Table 2-5. Model parameters related to the external source efficiency at the BOL.

	CERCER	CERMET	Nitride
Target radius, cm	39	39	22
Proton energy, GeV	0.8	0.8	0.8
Average energy of source neutrons, MeV	2.0	2.0	3.1
Proton source efficiency	11.0	9.0	19.8
Neutron source efficiency	0.54	0.45	0.95
Fissions per proton	128	98	199
Required proton current, mA	14.4	23.6	4.8
Proton beam power, MW	11.5	18.9	3.8
Energy gain	34	27	53

Table 2-6. Reactivity swing for the first irradiation cycle of 3 years.

	CERCER	CERMET	Nitride
k_{eff} swing, pcm	709	165	234
k_s swing, pcm	1,665	977	228
Ratio of swings	2.4	5.9	1.0
Proton current swing, mA	4.8	4.0	0.3

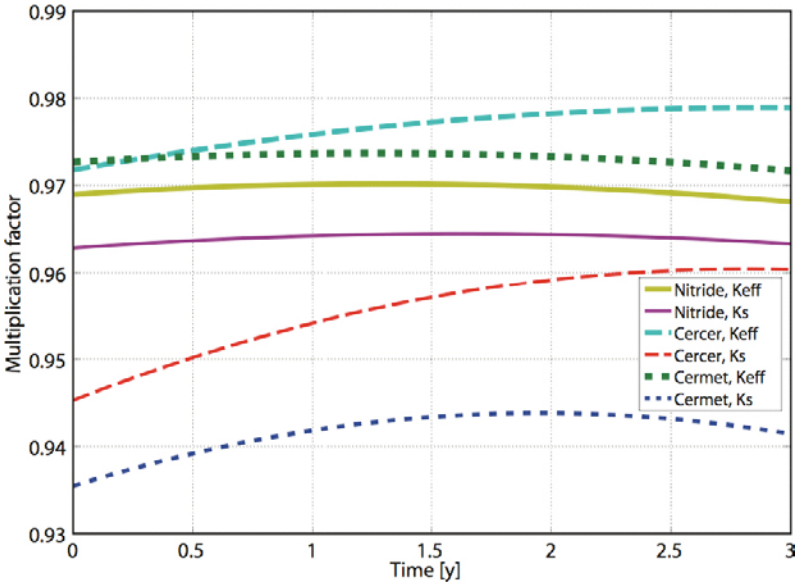

Figure 2-2. *Evolution of multiplication factors during burnup.*

The coolant void worth is calculated as the difference between k_{eff} with normal core conditions and k_{eff} of the core with the coolant removed around the fuel and between the fuel assemblies in the active zone. As seen in Table 2-7, the smaller core size and smaller coolant volume fraction contribute to a two times smaller coolant void worth of the nitride core compared to the reference CERCER core. In addition, a noticeable decrease (14–18%) of the void worth during 3 years of irradiation is obtained for all cores as a result of americium burn-up. The large amount of americium and strong dependence of its fission probability on the neutron spectrum /Tuček et al. 2004/ make Am to be the major contributor to the coolant void worth. The decrease of the void worth may allow increasing k_{eff} of the cores by 200–300 pcm per year improving economy of ADS operation. This can be implemented by a positive reactivity swing of matching value.

While the relative burnup of minor actinides (MA, namely Np, Am, and Cm) and all actinides in total (An) is similar for all cores (see Table 2-8), the absolute burn-up is essentially proportional to the total core power. It must be noted, that even if relative burning of minor actinides is higher for the CERCER core, the value may change when the reactivity swing is optimised to approach zero. Vice versa, if to adjust the nitride fuel composition for a higher fraction of MA to be transmuted, then the reactivity swing will be consequently shifted away from the current minimal value. By the EOC, a burn-up of 78.3 GWd/t (or 8.3% FIMA after 3 years of cooling) is achieved for all fuels. Evolution of Pu inventory during 3 years of operation and 10 years of cooling is presented in Figure 2-3. As one can see, the lowest Pu mass at the End-Of-Cycle (EOC) is followed by a significant build-up of Pu isotopes due to decay of Cm (Table 2-9, Figure 2-3) with the maximum value being reached in about 3 years of cooling. If this maximum value is desired to be equal to the initial Pu mass, i.e. if ADS is used for burning MA and keeping Pu for fast reactors, then one needs to tune the Pu/MA ratio with the consequences discussed above.

Table 2-7. Coolant void worth.

	CERCER	CERMET	Nitride
Void worth at BOL, pcm	7,077	6,244	3,504
Void worth at EOC, pcm	6,037	5,384	2,877
Void worth change, pcm	1,040	859	627
Void worth change, %	−15	−14	−18
Coolant volume fraction, %	58	54	43
Voided coolant volume, m^3	3.0	3.3	1.0
Fuel mass, ton HM	5.4	6.8	2.8
Am weight fraction change, %	–6.9	–6.6	–4.2

Table 2-8. Burnup characteristics after 3 years of operation and 3 years of cooling.

	CERCER	CERMET	Nitride
Total burnup, GWd/t	78.3	78.3	78.3
Relative burnup, % FIMA	–8.3	–8.3	–8.3
Relative mass change of Pu, %	–0.9	–0.3	–1.0
Relative mass change of MA, %	–14.7	–13.9	–14.2
Absolute mass change of An, kg	–439	–548	–232
Specific mass change of An, kg/TWh	–43.5	–42.8	–43.9
Specific mass change of An, kg/GWy	–381	–375	–385

Table 2-9. Actinide inventory in tons.

	Pu, t		Am, t		Cm, t	
	BOC	EOC	BOC	EOC	BOC	EOC
Nitride core	1.22	1.18	1.46	1.22	0.07	0.12
CERCER core	2.46	2.39	2.68	2.22	0.13	0.23
CERMET core	2.86	2.78	3.65	3.05	0.17	0.29

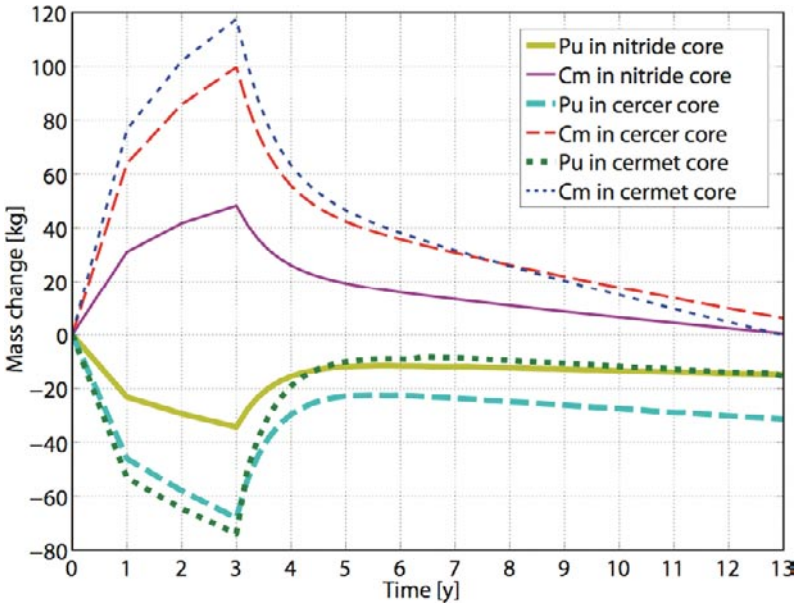

Figure 2-3. *Mass change of Pu and Cm.*

2.4 Conclusions

Neutronic and burnup parameters of EFIT core with three fuel options (CERCER, CERMET and nitride) have been calculated. It was shown that the reactivity swing of the CERMET core (EFIT-Mo/Pb) is minimized if the plutonium fraction in fissionable material is set to 42 at.% for the specific power of 71.5 MW/t_{HM}. Because of the worse neutron economy of CERMET fuel, the EFIT-Mo/Pb core requires larger amount of fuel and therefore larger core size, which decreases the efficiency of external source.

A compact EFIT core with nitride fuel (EFIT-N/PbBi) has been designed, based on the geometry of the EFIT-MgO/Pb core. It is shown that the good neutron economy of nitride fuel allows reducing the core size and therefore the total reactor power, while keeping the specific power constant, which then permits reduction of the spallation target radius. The smaller EFIT-N/PbBi core and smaller

spallation target area result in a significant increase of the proton source efficiency (by 80% compared to the CERCER core) and the neutron source efficiency (up to 0.95). Consequently, the proton current demand and the proton beam power decrease by 67%, which then decreases the heat deposit into the target and the load of the target heat removal. Additionally, much lower swings are achieved for both k_{eff} and k_s of the nitride core during the first cycle, providing conditions for safe and economical reactor operation. However, the reactivity swing optimization for the nitride and CERMET cores needs to be done for the equilibrium cycle as well.

Replacement of the ferritic steel T91 by the austenitic steel 15/15Ti in the EFIT-N/PbBi core allows reducing the pin pitch safely, which contributes to a reduction of coolant void worth by more than a factor of two. Decrease of the void worth by 200–300 pcm per year may allow a positive reactivity swing of a corresponding magnitude. The high matrix fraction (66–78 vol.%) of the nitride fuel in the EFIT-N/PbBi core leads not only to good thermal conductivity, but also gives a space for future design optimisation.

Despite the good characteristics of the nitride core, its low total power, the need in enrichment of nitrogen in N-15, and stability issues of the nitride fuel may decrease attractiveness of the proposed design. All three EFIT fuel candidates need further analysis before the optimal choice can be made based on their manufacturability, neutronic parameters, in-core behaviour, and economical efficiency.

3 Safety studies of ADS and Gen-IV systems

The major advantage of ADS is that it is much less sensitive to reactivity insertions, and hence may be loaded with large fractions of americium. Therefore it becomes a much more efficient burner of minor actinides than critical reactors of Gen-IV type. The upper limit of americium which may be present in the fuel of critical reactors have been quoted to reside in the range of 2–5%. However, a consistent study establishing well defined criteria for this limit has not been made available. Therefore, KTH has performed a parametric study of transient performance of a medium sized sodium cooled reactor loaded with varying fractions of americium in its MOX fuel.

The BN600 geometry was taken as a template for a model implemented in the SERPENT Monte Carlo code.

Neutronic parameters, including effective delayed neutron fractions (β_{eff}), Doppler constants (K_D), coolant void worths (W_{Na}/W_{LBE}) and axial/radial expansion coefficients (α_{ax}/α_{ra}) were obtained from the SERPENT calculations.

The SAS4A/SASSYS code (ver. 3.1) was then applied to simulate the safety behavior of the modelled sodium cooled reactor during ULOF and UTOP transients based on the safety parameters obtained from the SERPENT calculations, using an updated database of thermophysical properties of minor actinide bearing fuels.

Further, a full set of transient analysis was performed for the source efficient ADS with nitride fuel described in the preceeding section. The nitride fuel considered for the ADS had the composition $(Pu_{0.44}Np_{0.02}Am_{0.52}Cm_{0.02})N$ in solid soultion with ZrN in volumetric fractions of 70.0%, 63.0% and 52.5% in inner, intermediate and outer zones respectively

The thermal conductivites of the MOX and nitride fuels are displayed in Figure 3-1.

We may note the following:

1. The thermal conductivity of AmO_2 is more than 50% lower than that of UO_2.
2. The introduction of TRU nuclides will deteriorate the thermal conductivity of UO_2, especially when more than 15 at.% Pu or 3 at.% Am are introduced, mainly due to the effect of increased hypo-stoichiometry. The dependence on stoichiometry is more pronounced for americium oxide.

As shown in Figure 3-1, thermal conductivities of UN, NpN and PuN are 150%, 60% and 30% higher than that of AmN. A mixed nitride with large fraction of americium therefore will have a considerably lower conductivity than pure UN. In the case of the inert matrix fuel considered for the ADS here investigated, this is compensated for by the large thermal conductivity of ZrN.

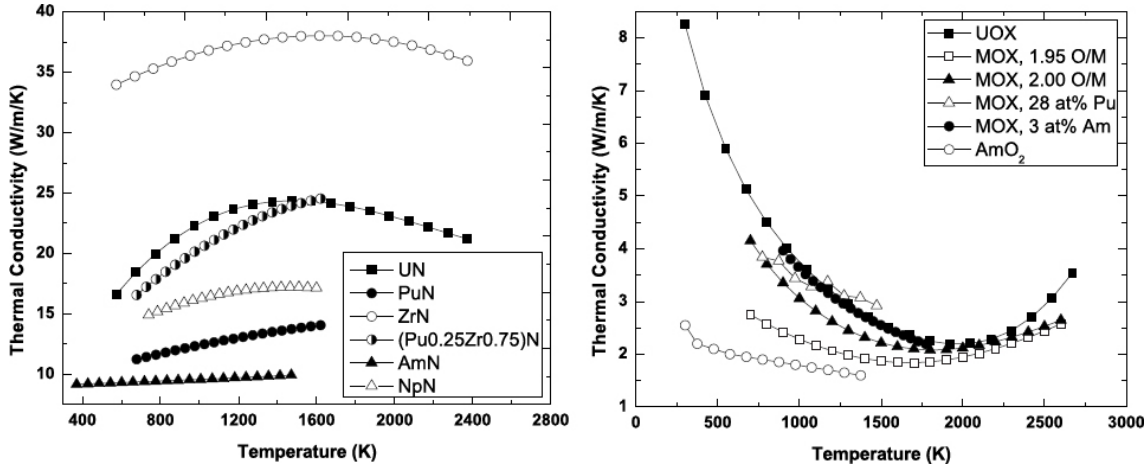

Figure 3-1. *Thermal Conductivities of AcN (left) and $AcO_{(2-x)}$ (right).*

3.1 Neutronic parameters

The introduction of Am into the fuel is known to be detrimental for Doppler feedback, coolant temperature coefficient, coolant void worth and the effective delayed neutron fraction. Figure 3-2 and Table 3-1 shows these safety parameters together with the calculated radial and axial expansion coefficients of the sub-assembly diagrid and the fuel. In Table 3-1, a "+" represents a benign effect and a "–" a malignant effect.

Table 3-2 displays the safety parameters calculated for the source efficient ADS with nitride fuel, compared to those of the reference EFIT designs.

Comparing to the reference designs of EFIT, the major merit of the new ADS design is a 60% smaller coolant void worth, thanks to its tighter pin lattice.

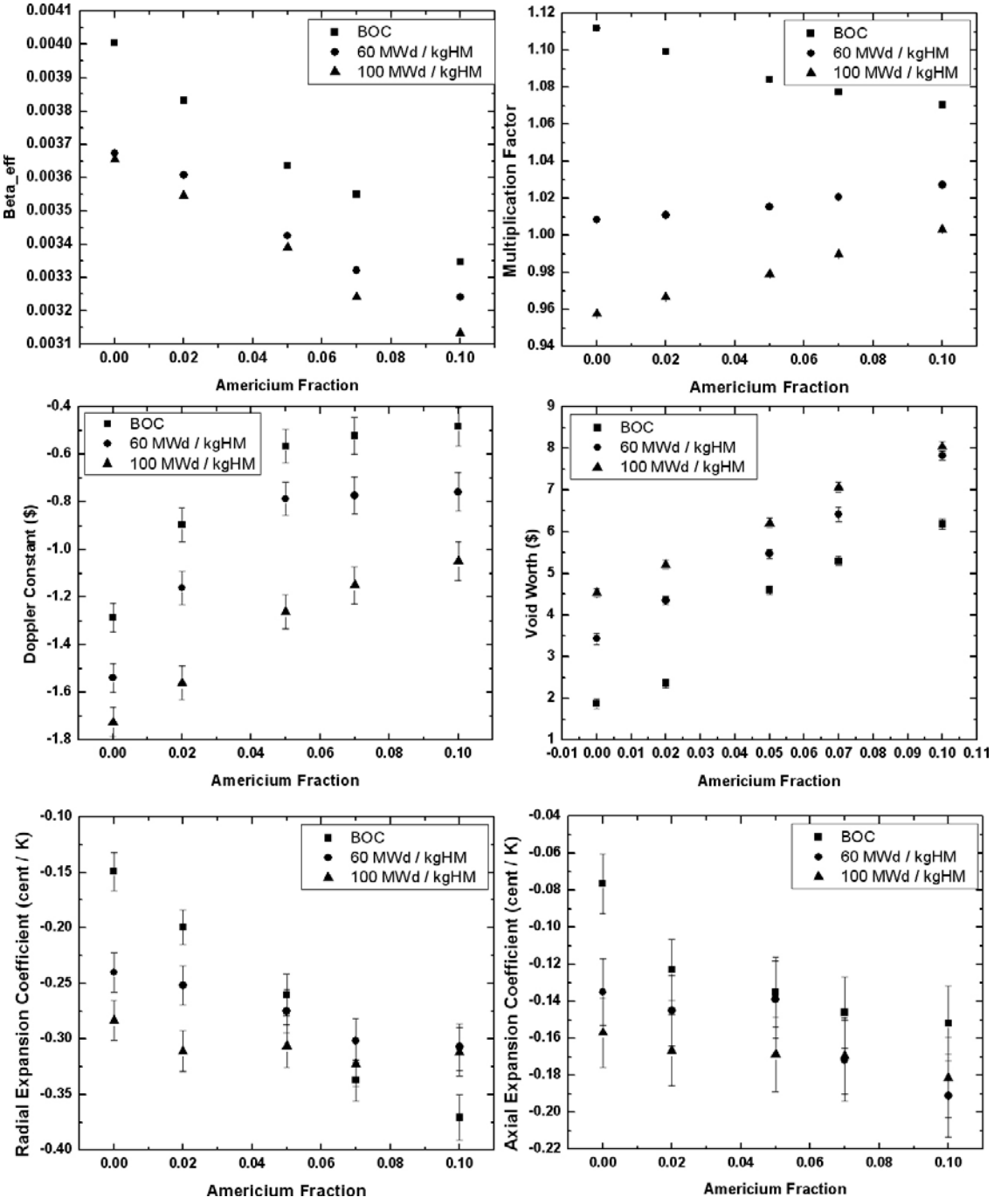

Figure 3-2. *Safety Parameters as function of Am content in fuel.*

Table 3-1. Summary of effects from introduction of Americium.

	β_{eff}	K_D	W_{Na}	α_{ra}	α_{ax}
BOL	–	–	–	+	+
EOEC	–	–	–	+	+

Table 3-2. Safety Parameters of different ADS designs, in units of pcm or pcm/K.

	β_{eff}	W_{LBE}	K_D	α_{ra}	α_{ax}
Nitride-ADS at BOC	167	3,585	9	0.55	0.14
Nitride-ADS at EOC	167	2,964	44	0.49	0.10
EFIT-400 CERMET, BOC	169	7,335	40	0.54	–
EFIT-400 CERCER, BOC	159	7,133	63	0.55	–

3.2 Transient simulation results

Simulations of postulated UTOP and ULOF transients showed that the most vulnerable component of the medium sized SFR design is the fuel, for which temperatures approach the melting point when the americium content is increased. Figure 3-3 shows the fuel temperature in the hottest channel during slow UTOP and ULOF transients, assuming a maximum linear rating of 37 kW/m.

As can be noticed, the fuel temperature at the hottest spot of fuel column will increase by approximately 300 K when Am content is raised from 1.0 wt.% to 5.0 wt.%. Cases with Am fraction higher than 3.0 wt.% will lead a fuel failure for the assumed linear rating of 37 kW/m. In order to accommodate the increase of fuel temperatures during the UTOP caused by reduced negative feedbacks, the power density under normal operation may be reduced. It was found that a power penalty of at least 6% results for each percent additional introduction of americium, in order to maintain a 100 K safety margin to fuel failure.

Figure 3-4 displays the results of transient simulations in the nitride fuelled ADS.

This ADS design hence can tolerate ULOF and UTOP transients with safety margins of 500 K, 150 K and 1,000 K for fuel, cladding and coolant respectively. The ULOF transient at BOC is the scenario with the smallest margins, during which temperatures of fuel, cladding and coolant can reach 1,900 K, 1,098 K and 927 K.

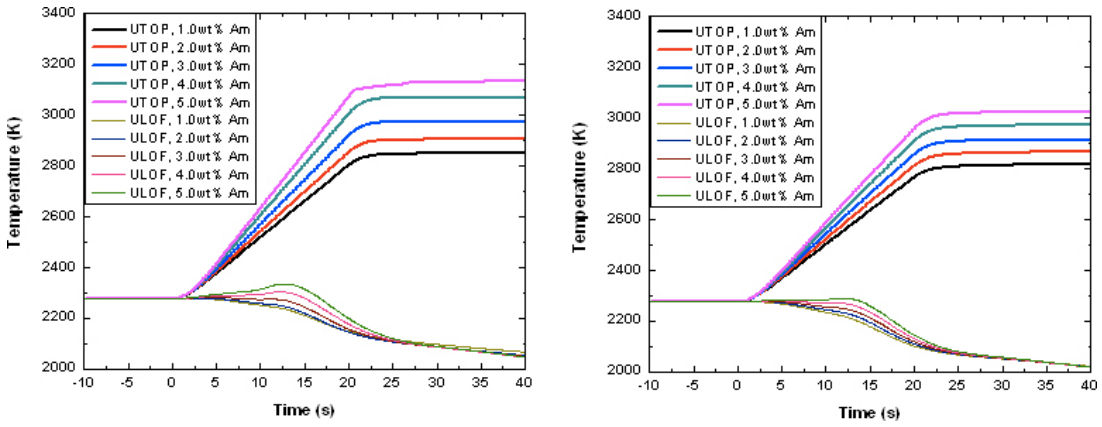

Figure 3-3. *Fuel Temperature during Slow UTOP and ULOF Transients at BOL (Left) and EOEC (Right),* P_{max}*=37 kW/m.*

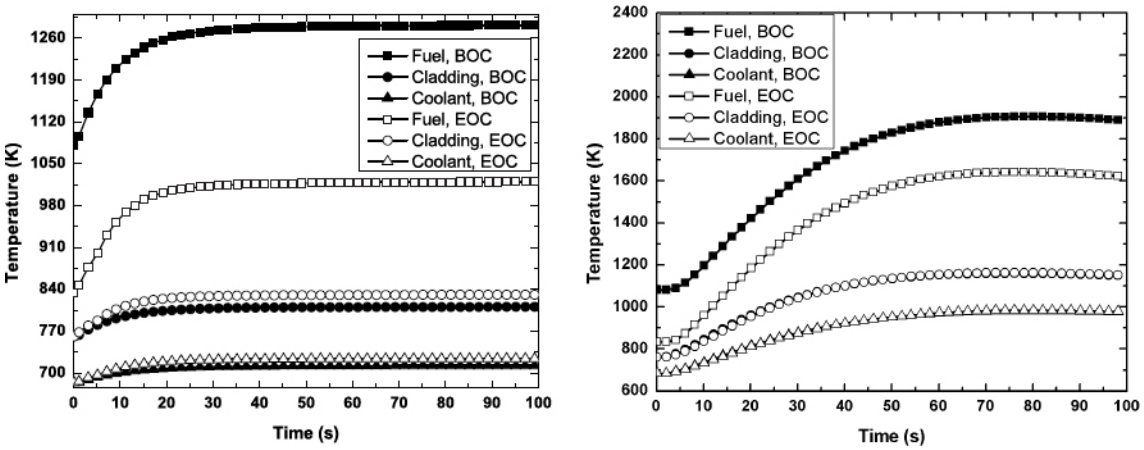

Figure 3-4. *Simulation of UTOP (Left) and ULOF (Right) transients in the ADS with nitride fuel.*

4 Sub-criticality monitoring

During 2009 data from four experimental campaigns at the coupled fast-thermal subcritical facility YALINA-Booster (Figure 4-1) have been analyzed in detail. The aim of the experiments has been to test and validate methods for reactivity monitoring and the most promising methods have been investigated within the framework of EUROTRANS /Knebel 2006/. A team of experimentalists from Sweden (KTH), Spain (CIEMAT), Germany (KIT and FZD), Portugal (ITN) and Poland (AGH) has jointly executed the experiments and analyzed a large set of data which constitutes an important part of the information needed in the process of defining a validated online reactivity monitoring methodology for planed future transmutation facilities such as XT-ADS and EFIT. The methods studied are

- the Sjöstrand area ratio method,
- the prompt decay method,
- the beam trip method,
- the Rossi-α method.

Some conclusions with respect to the above mentioned methods are presented below.

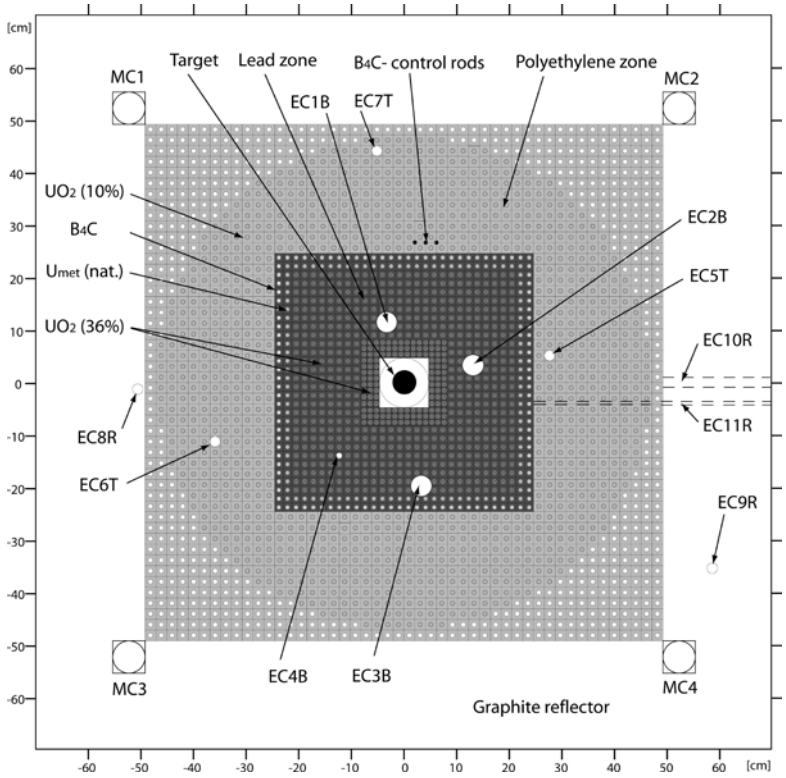

Figure 4-1. *Schematic cross-sectional view of the YALINA reactor core for the SC3a configuration.*

4.1 The Sjöstrand area ratio and prompt decay methods

By separating the total neutron density into prompt and delayed neutron densities and thereafter integrating over time, the prompt and delayed neutron areas, A_p and A_d, can be obtained /Sjöstrand 1956/. These areas are depicted in Figure 4-2 and it is straight forward to show that the reactivity in dollars is given by

$$\frac{\rho}{\beta_{eff}} = -\frac{A_p}{A_d}$$

The Sjöstrand area ratio method is the most carefully studied method of this work. The reason is its simplicity and that it has shown a high degree of stability in previous studies /Rosa 2007, Jammes 2006/. The fact that the observables are integrals makes the method attractive in an accuracy perspective. An important requirement when applying this method is that the fundamental mode overwhelms all other possible modes. However, as will be shown here, there is practically always a contribution from other modes, thus causing what is referred to as spatial dependence.

The reactivity can also be obtained from the decay rate of prompt neutrons, given by /Simmons and King 1958/:

$$\alpha = \frac{\rho - \beta_{eff}}{\Lambda}$$

Using the Sjöstrand area ratio method, it was found, that the reactivity as measured in the fast zone could deviate almost 100% from the value obtained in the thermal zone. The explanation is, on one hand, the very strong source mode in the fast zone data, which can be seen in Figure 4-3, and, on the other hand, the fact that the fast and thermal zones have different spectra and are partly decoupled. Based on a two-region point kinetics model it can be shown that the estimated global area ratio reactivity is, for the fast and thermal zone respectively, given by

$$\rho_{\$1} = -\frac{A_{p1}}{A_{d1}} \approx \frac{\rho_2}{\beta_2}\left(\frac{1}{f}\alpha_1\tau_1\alpha_2\tau_2 - 1\right) + 1$$

and

$$\rho_{\$2} = -\frac{A_{p2}}{A_{d2}} \approx \frac{\rho_2}{\beta_2}\left(1 + f\frac{1}{\alpha_1\tau_1}\right) - f\frac{1}{\alpha_2\tau_2\beta_2}$$

In these equations, subindex 1 refers to the fast zone and 2 to the thermal zone, τ is the mean neutron lifetime and f is the return probability describing the probability of a neutron to leave a region and later come back again. The equation above indicates that for both regions, the measured value of the global reactivity is based on the reactivity of the thermal zone with a term and factor describing the coupling of the fast zone. Thus, the ratio of the area ratio reactivities of the two zones depends heavily on the return probability.

Converged reactivity values could finally be obtained after applying correction factors obtained through Monte Carlo simulations. These correction factors were obtained by calculating the prompt and delayed fluxes at the detector positions in source mode and by normalizing them to the effective multiplication factor from the criticality calculation. In this way a correction giving directly the experimental effective multiplication factor was obtained without the need of explicitly calculating the effective delayed neutron fraction.

Applying the prompt decay method gave much more stable results. The only deviation could be found in the reflector at deep subcriticalities. Thus, this method has a clear advantage over the area ratio method.

An investigation of the possible k_s dependence of the area ratio method was performed. The parameter k_s describes the multiplication of the source neutrons in contrast to k_{eff} which describes the multiplication of the fission neutrons. Following long discussions within the community it was decided to have in the YALINA-Booster experiments two configurations having the same k_{eff} but different k_s.

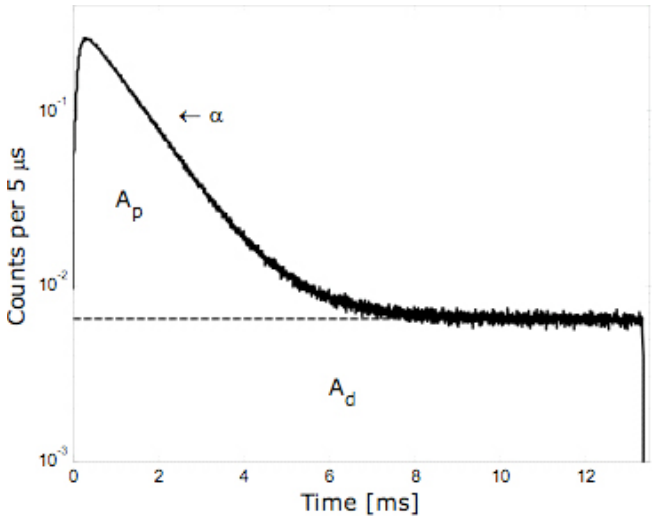

Figure 4-2. *Prompt and delayed neutron areas used in the area method, as well as the exponential decay of prompt neutrons (time discretization 5 μs).*

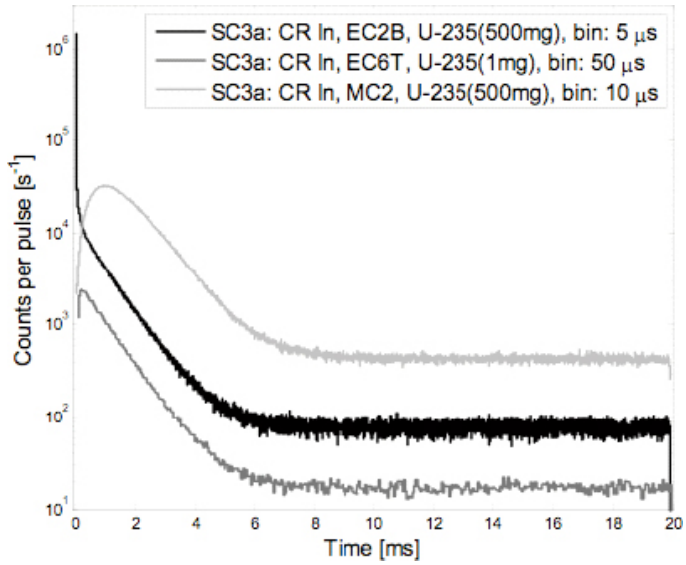

Figure 4-3. *PNS histograms for configuration SC3a (CR inserted).*

This could be achieved by removing highly enriched fuel from the core centre, close to the neutron source, and compensating by adding low enriched fuel at the core periphery. It could finally be concluded that a change in k_s of about 500 pcm did not have any visible effect on the Sjöstrand area ratio reactivity.

4.2 The Beam Trip Method

Assuming a subcritical core at constant power driven by an external source, a neutron flux level somewhere in the core will be n_0. Suddenly, the external neutron source is shut-down or removed very quickly. Then, the neutron flux changes rapidly to a semi-stable level n_1. In the same manner as for the Sjöstrand area ratio method it can be shown that the reactivity in dollars is given by

$$\frac{\rho}{\beta_{eff}} = \frac{n_1 - n_0}{n_1}$$

When the method is applied in this way it is referred to as the source jerk method. In the YALINA-Booster experiments it was possible to apply this technique in a repeated manner with a constant frequency of 1 Hz and with a beam interruption time of about 30 ms. When applying the method in this way, one must remember that the prompt neutron density recovers directly when the source is restarted, whereas the delayed neutron density is reduced compared to the constant source equilibrium case. Therefore, a correction must be applied that takes into account this effect. The correction factor of n_1 is to a good approximation simply the total flux as if there was no beam interruption divided by the observed total flux with beam interruption. The absolute value of the correction is added to n_0 and n_1 before evaluating the reactivity.

Before the experimental work started, the control module of the neutron generator was modified to allow current mode operation with short interruptions (beam trips) and with a trigger signal to the data acquisition system for synchronization. In this way thousands of beam trips could be accumulated to obtain the reactivity with low statistical uncertainty. With the beam operating in current mode, a strong oscillation of the flux was observed. The same oscillation could be found in the beam current, but with lower relative amplitude. The oscillation had a frequency of 50 Hz and was a disturbance from the electricity grid that could not easily be eliminated. The oscillation affected the bending magnet in the beam line and caused the beam impact position on the target moving. Each cycle the beam hit the target close to the boundary were the tritium concentration is lower. Nevertheless, since the oscillation appeared in the ms-scale and it was not present during the trips it did not affect the results of the experiments. The signal from the beam current meter and the fission chamber in the booster region are displayed in Figure 4-4. The oscillations are clearly visible before the beam trip in both the beam current and the detector. The beam current carried additional high-frequent noise that is visible also after the beam trip. In the same figure, the delayed neutron flux, n_1, is clearly visible after the beam trip at $t = 0$. The total flux level, n_0, must be obtained as an average over an integer number of beam oscillation periods.

An example of beam trip histograms are shown in Figure 4-5, in which nearly 1,000 beam trips have been accumulated. When data are added to each other, the oscillations tend to decrease or get deformed due to destructive interference, but it does not affect the results as long as the average value is taken over an integer number of oscillation periods. In the figure, the effect of the control rods can be seen as lower count rate in the detector. By plotting in logarithmic scale, the effect on the prompt decay constant can be viewed (right pane). It has been shown that the same results can be obtained from the beam trip histograms as from the pulsed neutron source histograms, including the same spatial spread. Thus, having high enough count rate it is possible to use this method as an online reactivity meter. This was tested in these experiments, although the count rate was in the lower range to obtain the reactivity with high enough statistical accuracy.

In Figure 4-6, the reactivity was measured once per second using the beam trip method while extracting the control rods during $0 < t < 5$ s. Despite the high uncertainty in each data point, the reactivity increase can be tracked by this method. However, a clear disadvantage of this method

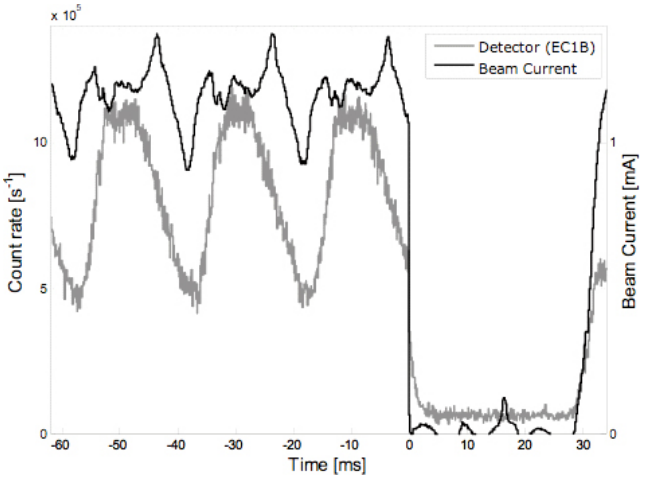

Figure 4-4. *Detector count rate in EC1B (grey) before and during a beam trip (beam current in black).*

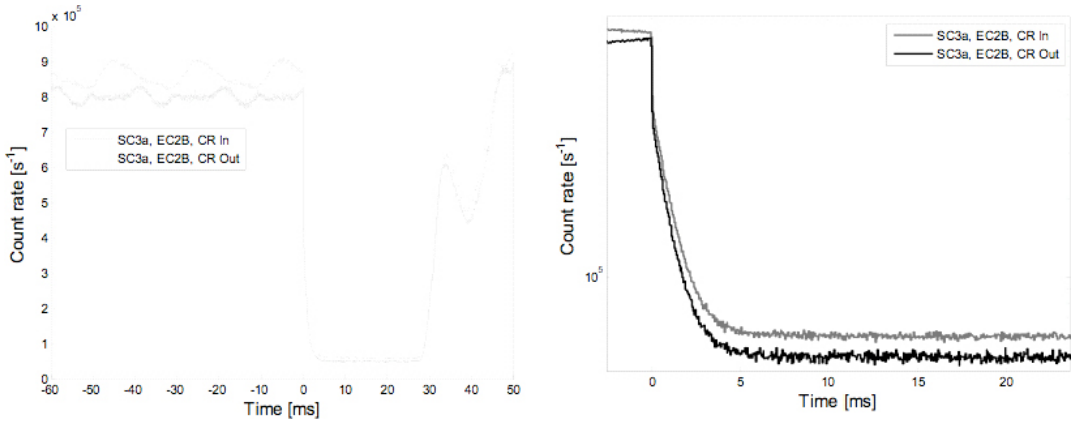

Figure 4-5. *Beam trips histograms of SC3a, detector location EC2B for the two cases with control rods inserted and withdrawn (linear and logarithmic).*

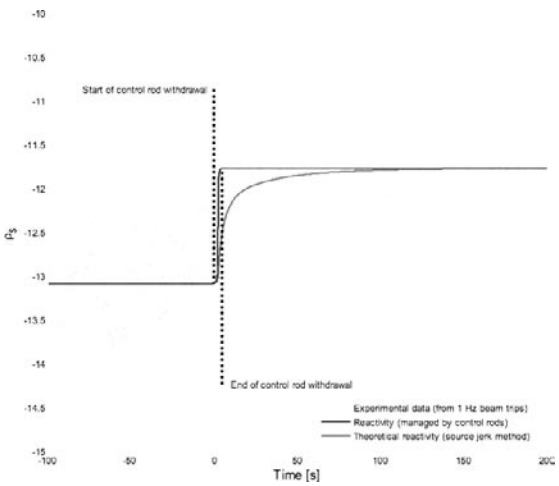

Figure 4-6. *Reactivity monitoring with the beam trip technique.*

is the long stabilization time of the beam trip reactivity. Since it requires that the equilibrium level of the delayed neutrons has been reached, it takes about two minutes to stabilize at the new value. This theoretical reactivity, given by the point kinetics equations is given in grey in the same figure. Important is to point out that during the transition period, the measured reactivity over-estimates the margin to criticality, which is a major drawback. Therefore, it would be better to base the reactivity monitoring on the prompt decay constant measured after each beam trip.

4.3 The Rossi-α Method

Due to the fission chain reactions in a multiplying medium, detected neutrons may be correlated to each other in space and time. It might happen that two neutrons, detected by the same neutron detector, originate from the same fission chain. In such case, it is likely that these two detections, or events, are close in time. It can be shown that the probability to detect one more neutron after the first neutron decreases exponentially in time with the prompt neutron decay constant α. The probability density function is given by

$$p(t)dt = -\frac{\varepsilon D_v}{2\alpha\Lambda^2} e^{\alpha t} dt + F\varepsilon dt$$

with the random events included and the common parameters introduced /Kistner 1964/. The study was limited to the thermal zone, since the count rate was too low in the fast zone to obtain useful results, even with the largest detector and the strongest neutron source available. The experimental

data from the thermal zone revealed not less than three alpha-modes present in the auto-correlation (Figure 4-7). Dual alpha-modes have been reported previously in reflected systems where the core and the reflector contribute with one alpha-mode respectively /Kuramoto 2007, Spriggs 1997/. In the case of YALINA-Booster, there is an additional fast alpha-mode originating from the booster zone. The presence of the higher alpha-modes causes some limitations in the use of the Rossi-α method. First of all, most of the correlated part of the histogram is occupied by the higher alpha-modes. Thereby, the slowest decaying alpha-mode is best viewed close to the uncorrelated background. Thus, obtaining results with high accuracy is challenging and extremely long measurement times are needed. In addition, having alpha-modes close to each other causes larger uncertainties from the fitting error estimation. In the end, it was not possible to follow a reactivity perturbation of 0.5 $ even after several hours of measurements.

Another interesting observation is that the value of the higher alpha-modes is much less reactivity dependent compared to the slowest alpha-mode. The fastest alpha-mode could to a very good approximation be assumed constant at least in the subcriticality interval 0.85–0.977. The same holds for the first higher eigenmode except at deep subcriticality. It gives an indication that the higher eigenmodes are driven by the surrounding geometry and materials rather than the amount of fuel loaded.

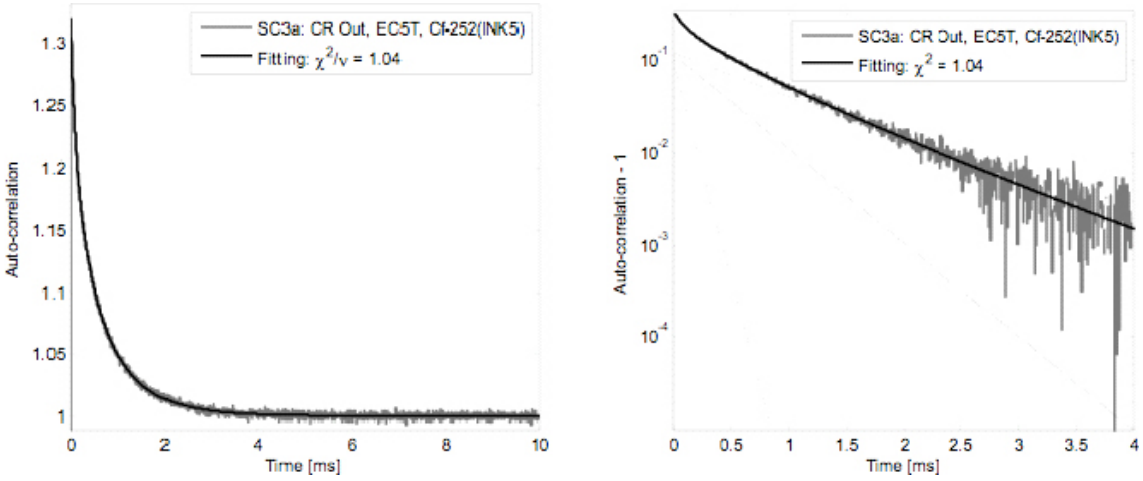

Figure 4-7. *Rossi-α histogram and fitting in linear and logarithmic scale (5 μs time bin). The contribution from individual exponentials is indicated by dashed lines.*

5 Neutron cross section measurements

Neutron elastic scattering cross-section has been measured in cooperation with the Uppsala University department of Applied Nuclear Physics at the Theodor Svedberg Laboratory (TSL), Uppsala. Under the year 2009, two experimental runs were performed acquiring data for lead and bismuth targets and for silicon in the other run. The data has been obtained using the SCANDAL set-up.

Protons accelerated to 179.3 ± 0.8 MeV by the Gustaf Werner cyclotron impinge on a neutron production facility at TSL. The facility utilizes a 23.5 mm thick lithium target, enriched to 99.99% in ^{7}Li, and the ^{7}Li(p,n)^{7}Be reaction to create a quasi-monoenergetic neutron spectrum consisting of a high-energy peak and a low-energy tail. The average neutron energy in the peak is 175.0 MeV and the width of the peak is approximately 5 MeV. The peak contains about 40% of all neutrons. A neutron beam is formed by a set of collimators and creates a circular beam spot with a diameter of 8.2 cm at the scattering target position.

5.1 The SCANDAL set-up

The SCANDAL set-up consists of two arms that can be rotated around a pivot point where the scattering target is located. Both arms are geometrically identical. Each arm is equipped with four plastic scintillators: a veto, a converter and triggers 1 and 2. The veto and both triggers consist of 2 mm thick plastic scintillators. The veto is used for fast charged-particle rejection, so in a standard neutron detection mode, a trigger condition to read out the system consists of a coincidence between the triggers 1 and 2 vetoed by the front plastic scintillator. Since it is not possible to detect neutrons directly, conversion to a charged particle (e.g. a proton) is desirable. The neutron-to-proton converter in SCANDAL is a 20 mm thick plastic scintillator ($C_1H_{1.102}$). Using an active converter allows the proton energy loss within the converter to be measured and compensated for. An array of eight scintillators at the back side of each arm is intended to stop the protons so that their full energy is deposited. The scintillators are 9 cm deep, 8 cm wide and 22 cm high crystals made of CsI(Na). They are counted from the left as CsI 1 to CsI 8 on the left arm and CsI 9 to CsI 16 on the right arm. Two drift chambers are positioned between triggers 1 and 2 at both arms. The drift chambers provide information about proton trajectories, so the neutron-to-proton conversion point inside the converter can be determined and simply related to the scattering angle of the original neutron. The layout of the scintillators and the drift chambers is depicted in Figure 5-1.

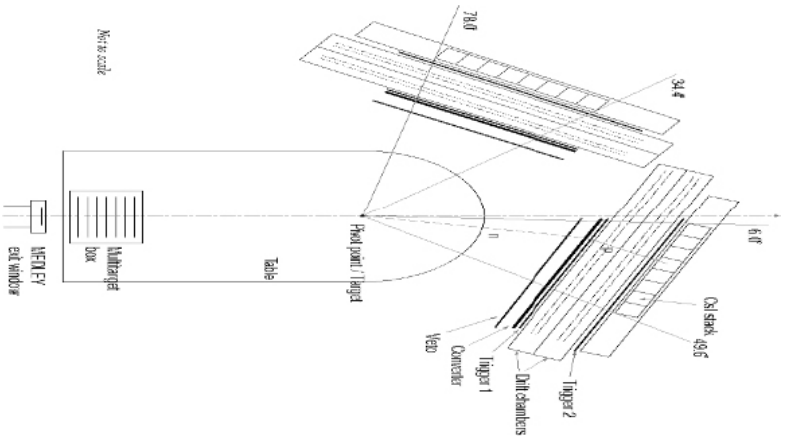

Figure 5-1. *Schematic view of the SCANDAL set-up in one of the configurations. Here the right arm is as close as possible to the beam with CsI 9 yet outside the beam.*

To be able to better understand the raw data obtained from the experimental runs and to prepare for the upcoming of-line data analysis a series of Monte Carlo calculations have been performed. For this purpose, MCNPX 2.7.A was utilized. Employing the mix-and-match option of MCNPX, the data libraries were used up to the maximum energy and models were used for higher energies.

5.2 CsI spectra in dependence of the conversion angle

To be able to distinguish whether the neutron was converted to the proton on hydrogen or carbon, a clear separation of the hydrogen and the carbon peaks in the proton spectrum is required. The energy of the proton with a conversion angle of 15.2° is lowered exactly by 12.6 MeV compared to the neutron. Thus, to distinguish the conversion on hydrogen from the conversion on carbon, the conversion angle has to be smaller than 15.2°.

5.3 Hit position gates

The protons which enter one of the CsI crystals close to one of the two lateral faces have a probability to escape from the crystal and thus deposit only part of their energy in one crystal. The off-line selection of suitable events could be done by imposing a hit position gate, which is smaller than the front surface of the crystal.

Results of the simulations are expressed as the proton leakage through a lateral face (in percent; as a fraction of all protons entering the crystal). The leakage is a function of a proton slit width which defines the hit position gates. The leakage is compared for each CsI crystal in Figure 5-2.

5.4 The Converter

The energy deposited by protons inside CsI 5 is depicted in Figure 5-3. This figure exhibits also the respective contributions of carbon and hydrogen in the converter to the conversion process. The data was obtained from separate calculations and the original converter was replaced by an imaginary converter made of pure hydrogen and pure carbon respectively.

A simulation-based neutron-to-proton conversion efficiency of the converter is $5.1\ 10^{-4}$. The conversion efficiency can also be calculated by comparing the area of hydrogen atoms as seen by the neutron to the real area of the converter. In that case, the efficiency would be equal to $5.5\ 10^{-4}$. This simplified theoretical calculation thus confirms that the result obtained from the simulation is reasonable.

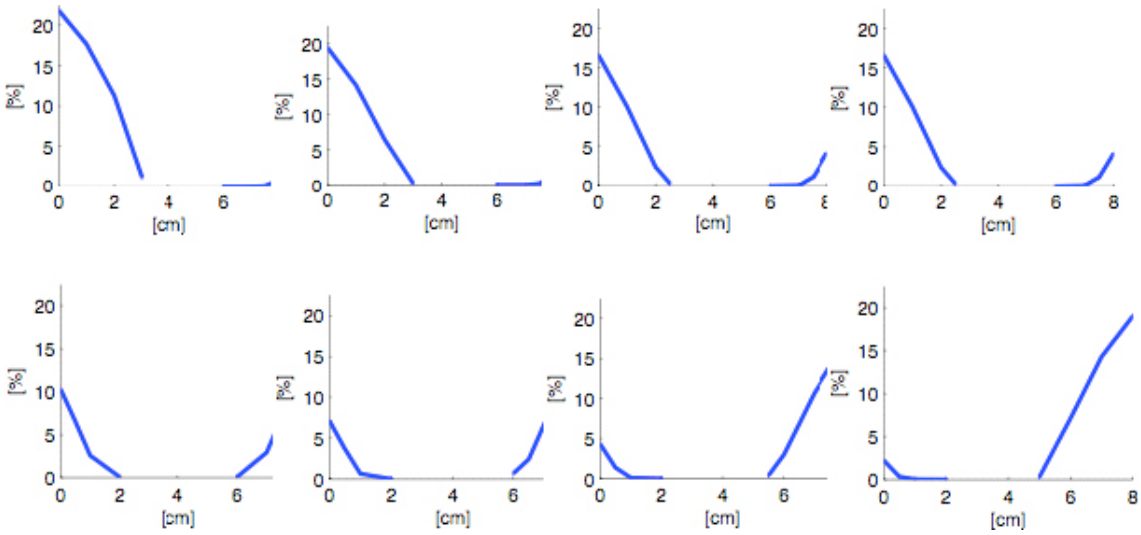

Figure 5-2. *Proton leakage as a function of the hit position gate for CsI 1 to CsI 8. Each X-axis represents opening of the entrance slit compared to the full width of a crystal (i.e. 8 cm). The Y-axis shows the percentage of protons escaped through the left and right sides respectively.*

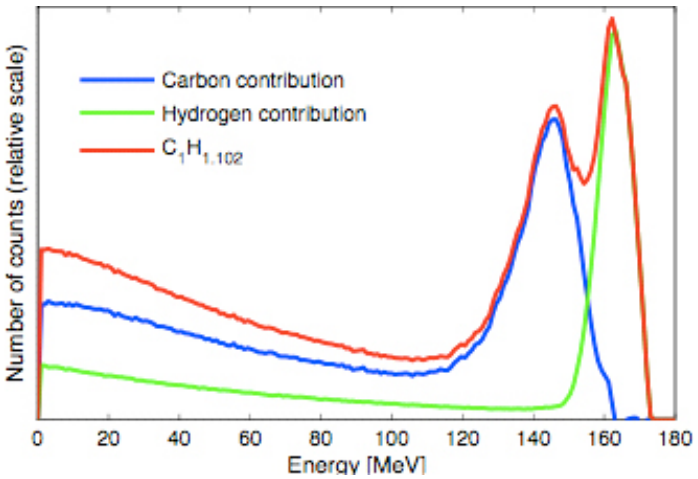

Figure 5-3. *Proton energy deposited in one of the crystals showing respective contributions of hydrogen and carbon to the neutron-to-proton conversion.*

6 Fuel laboratory

6.1 Introduction

A laboratory for manufacture and testing of small quantities of novel nuclear fuel materials (tens of pellets per batch) has been built and brought into operation. The facilities allow production of uranium nitrides as well as inert nitrides to be used as additives to improve the physical and chemical properties of the fuel. The selected method of synthesis (hydridation-nitridation of pure metal) results in very fine uranium powders of very fine grain size and, unlike the more common route starting from oxide material, it eliminates oxygen or carbon impurities in the product.

In literature there exists quite a lot of information about this method for synthesising uranium nitride, as it was at that time the most commonly used for production of uranium nitride. There is less data regarding the production of zirconium nitride by the same method.

As the nitride powders are sensitive to air and humidity, powder handling is performed in glove boxes under inert atmosphere.

6.2 Synthesis of fuel materials

The reaction conditions were investigated by TGA (thermogravimetric analysis) in order to find the most suitable combination of reaction times and temperatures. Our starting materials for the analysis were metallic uranium and reactor-grade (hafnium-free) sponge zirconium. Typical sample weights were 200–700 mg. One initial issue was the choice of crucible material, as there were concerns regarding alumina crucibles reacting with our samples at high temperatures. After testing and not finding any visible reaction with our samples, we decided to use alumina crucibles for the TGA measurements.

Figure 6-1. *Glove box installed in the uranium laboratory at KTH.*

The TGA experiments have more or less confirmed what is reported in literature. At about 250°C, in hydrogen gas, metallic uranium is converted to a fine, greyish powder. The following nitridation proceeds with a high reaction rate at 350–400°C resulting in the sesquinitride (U_2N_3). By an immediately following denitridation step at 1,200°C, uranium mononitride (UN) was formed as a gray-yellow fine powder. With an ordinary optical light microscope, the powder size could be roughly estimated between a few µm up to at most 50 µm, which was considered sufficiently fine for the first pellets pressing experiments.

In order not to waste uranium, the first preparative-scale experiments were performed with zirconium. In contrast to uranium, zirconium does not break down to powder during hydridation, for which reason the following reaction with the nitrogen is not facilitated to the same extent. One option is to mill the now brittle zirconium hydride before the next step of synthesis, but that poses some problems with increased contamination by oxygen in transfer from the furnace. Nitridation of ZrH_2 with and without previous milling has been performed. The product is generally of a good quality (see XRD results) but with both methods there have been some indications of residual metallic zirconium, which is very surprising from a theoretical point of view.

Uranium nitride synthesis indeed results in very fine powders of high purity, and no further improvement to the methods appears necessary.

6.3 Pellet pressing

The produced powders are mixed and further comminuted in nitrogen or argon atmosphere in a hermetically sealed shaking-cup homogeniser, after which pellets are pressed in a manually operated hydraulic press in another glove box. The effect of pressing and sintering aids will be systematically investigated.

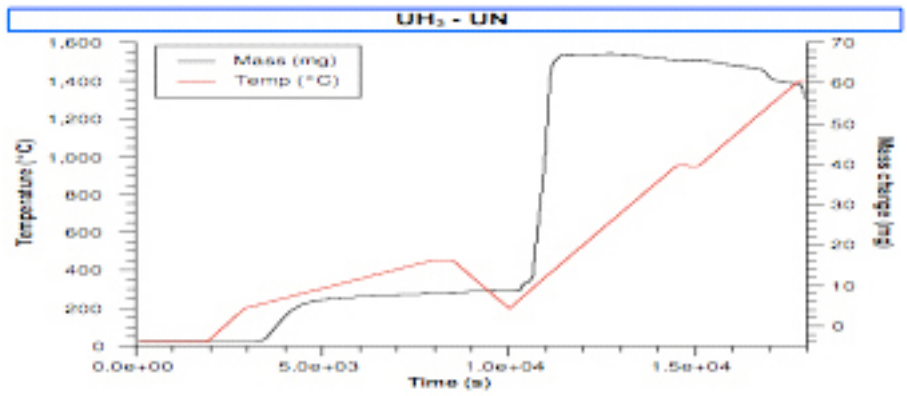

Figure 6-2. *Conversion of uranium hydride to nitride.*

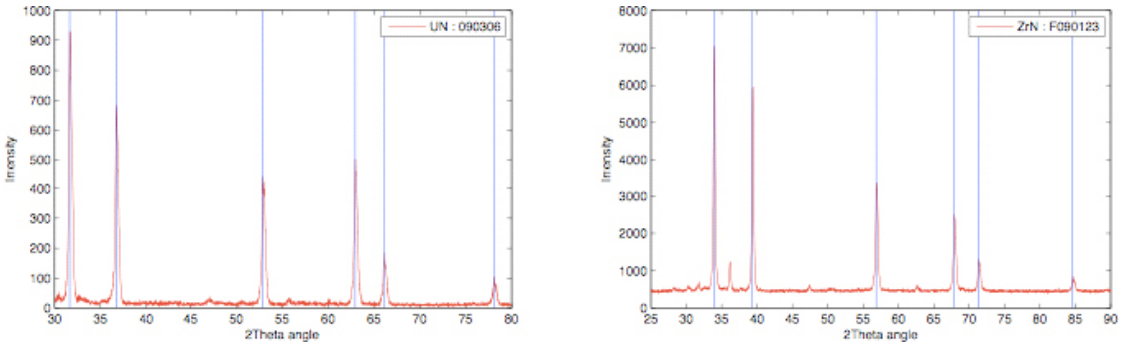

Figure 6-3. *XRD spectra of UN and ZrN powders.*

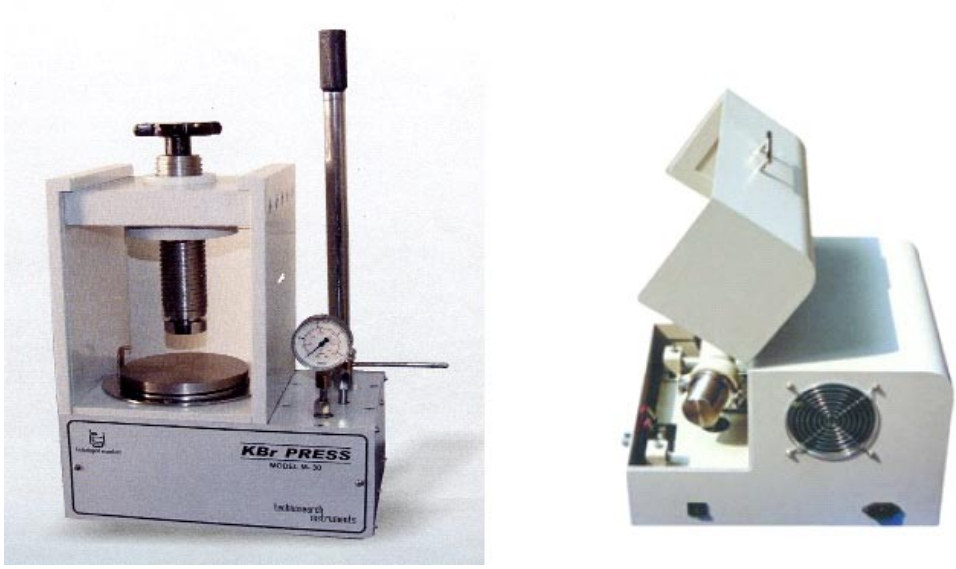

Figure 6-4. *Pellet press (left) and powder mill (right).*

6.4 Sintering of pellets

Uranium nitride sinters at a higher temperature than conventional oxide fuels. Additives that may be used for stabilising the fuel, e.g. zirconium nitride, may further raise the sintering temperature. Also, maintaining a controlled, inert or slightly reducing atmosphere during sintering is essential. Even small amounts of oxygen could severely lower the quality of the product.

We have therefore purchased a custom-made sintering furnace operating at temperatures up to 2,000°C. A number of test-runs revealed unexpected electrical interference between the driving current and the temperature sensor, apparently due to rapidly increasing electrical conductance of the boron nitride ceramic at high temperatures. The thermocouple will be replaced with an improved design after which sintering experiments will continue.

In parallel with conventional sintering, we have investigated the potential usefulness of SPS (Spark-Plasma Sintering) technology. In a test run, ZrN pellets of 93% TD were obtained. Manufacture of the first series of UN and (U,Zr)N pellets with use of this technique is scheduled for April 2010.

Figure 6-5. *High-temperature sintering furnace.*

Figure 6-6. *Unpolished ZrN pellets sintered by the SPS technique.*

6.5 Analysis of pellets

Green and sintered pellets have been analysed by scanning electron microscopy (SEM). The pellets were prepared by grinding and then polishing the pellets with diamond paste. The SEM pictures of pure ZrN pellets sometimes show metallic inclusions of up to 500 µm. Attempts were made to solve this by trying to modify the synthesis parameters, e.g. using longer reaction times .The problems persisted and we have at the time being introduced sieving to eliminate such inclusions. By sieving the milled ZrN powder down to below 70 µm the problem seemed to be solved with almost no visible metallic inclusions in the SEM pictures.

We have also procured commercial ZrN powder of high purity for comparison, and will in time decide upon whether to use our own ZrN or rely on commercially available material.

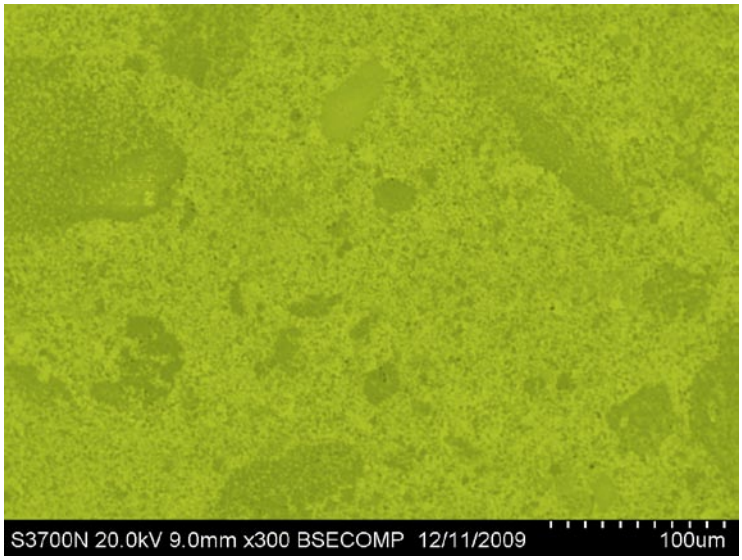

Figure 6-7. *SEM image of ZrN pellet, revealing some inhomogeneity.*

6.6 Chemical compatibility tests

The dense sintered pellets will be used for – among other things – studies of their compatibility with conventional and advanced coolants (water and lead alloys, respectively). High-temperature tests in water and steam will result in very high pressures. A design for a test capsule has been developed and a prototype has been built at a KTH workshop. The prototype performed excellently in a test run at 350°C and 170 atm pressure.

The resistance to dissolution in water under conditions mimicking those in a geological repository is also of some interest. Test at lower temperatures in an externally irradiated water bath can be performed already this year. We have been invited to use already existing facilities at KTH for these tests.

Tests in liquid lead alloys are also planned but will require installation of some new equipment, which however is not very complicated or expensive (a dedicated induction oven with protective gas environment).

Figure 6-8. *Autoclave for test of (U,Zr)N compatibility with water under LWR conditions.*

7 References

Arai Y, Akabori M, Minato K, 2006. JAEA's activities on nitride fuel research for MA transmutation. In Proc. 9th OECD/NEA IEMPT, Nîmes, France.

Arai Y, Akabori M, Minato K, Uno M, 2008. Development of Nitride Fuel and Pyrochemical Process for Transmutation of Minor Actinides. In Proc. 10th OECD/NEA IEMPT, Mito, Japan.

Artioli C, Glinatsis G, Petrovich C, Sarotto M, 2008. Specification for the EFIT Core and Fuel Element. Delivery report D1.6, EUROTRANS.

Cannon N S, Huang F H, Hamilton M L, 1992. Transient and static mechanical properties of D9 fuel pin cladding and duct material irradiated to high fluence. ASTM Special Technical Publication pp 1071–1082.

Cetnar J, Gudowski W, Wallenius J, 1998. MCB: a continuous energy Monte Carlo burnup simulation code. In Proc. 5th OECD/NEA IEMPT, Mol, Belgium, OECD/NEA, p 523.

Chadwick M, Hughes H, Little R, Pitcher E, Young P, 2001. Nuclear data for accelerator-driven systems. Progress in Nuclear Energy, Vol 38, pp 179–219.

Dulla S, Cadinu F, Picca P, Ravetto P, 2006. Effects of neutron source characteristics in direct and adjoint problems for subcritical systems. International Journal of Nuclear Energy Science and Technology, Vol 2, pp 361–377.

Fokau A, Zhang Y, Ishida S, Wallenius J, 2010. A source efficient ADS for minor actinides burning. Annals of Nuclear Energy, Vol 37, pp 540–545.

Golovanov V N, Kryukov F N, Kuzmin S V, 2006. Results of post-irradiation examinations of nitride and inertmatrices fuels irradiated in BOR-60 reactor. In Working Material of an IAEA Technical Meeting in Obninsk (Russia), November 21–23, 2005, Vienna (Austria), IAEA, pp 740–778.

Henry J, 2009. Structural and Cladding Materials for GEN-IV Sodium Cooled Reactors. In Proc. MATGEN-IV.2 winter school, Jukkasjärvi, Sweden.

Hilton B, Porter D, Hayes S, 2006. Postirradiation examination of AFCI nitride and oxide transmutation fuels at 8 at.%. In Transactions of the American Nuclear Society, pp 777–779.

Jammes C, 2006. Absolute Reactivity Calibration of Accelerator-Driven Systems after RACE-T Experiments. Proc. of PHYSOR 2006, Vancouver, BC, Canada.

Kistner G, 1964. Rossi-α theory for assemblies with two prompt neutron groups. Nukleonik Vol 7, No 2, pp106.

Knebel J, 2006. European Research Programme for the Transmutation of High Level Nuclear Waste in an Accelerator Driven System. In Proc. FISA 2006.

Koning A, Forrest R, 2006. The JEFF-3.1 Nuclear Data Library. OECD/NEA.

Kuramoto R Y R, 2007. Absolute measurement of β_{eff} based on Feynman-α experiments and the two-region model in the IPEN/MB-01 research reactor. Annals of Nuclear Energy, Vol 34, pp 433–442.

Maschek W, Artioli C, Chen X, Delage F, Fernandez-Carretero A, Flad M, 2008a. Design, safety and fuel developments for the EFIT accelerator driven system with CERCER and CERMET cores. In 10th IEMPT, Mito, Japan, OECD/NEA.

Maschek W, Chen X, Delage F, Fernandez-Carretero A, Haas D, Matzerath Boccaccini C, 2008b. Accelerator driven systems for transmutation: Fuel development, design and safety. Progress in Nuclear Energy, Vol 50, pp 333–340.

Mashnik S, Sierk A, Gudima K, Baznat M, 2006. CEM03 and LAQGSM03 – New modelling tools for nuclear applications. Journal of Physics: Conference Series, Vol 41, pp 340–351.

Minato K, Takano M, Otobe H, Nishi T, Akabori M, Arai Y, 2009. Thermochemical and thermo-physical properties of minor actinide compounds. Journal of Nuclear Materials, Vol 389, pp 23–28.

Nishihara K, Iwanaga K, Tsujimoto K, Kurata Y, Oigawa H, Iwasaki T, 2008. Neutronics design of accelerator-driven system for power flattening and beam current reduction. Journal of Nuclear Science and Technology, Vol 45, pp 812–822.

Pelowitz D B, Hendricks J S, 2008. MCNPX 2.7.A Extensions. Los Alamos National Laboratory.

Pillon S, Wallenius J, Smith P, Maschek W, 2003. The European FUTURE Programme. In Proc. Global 2003, New Orleans, LA, USA.

Pillon S, Wallenius J, 2006. Oxide and nitride TRU fuels: Lessons drawn from the CONFIRM and FUTURE projects of the 5th European Framework Program. Nuclear Science and Engineering. Vol 153, pp 245–252.

Rosa R, 2007. RACE-T Experimental Activities – A Complete Overview of the Different Subcritical Measurement Techniques. Proc. of Int. Conf. AccApp'07, Pocatello, ID, USA.

Saito S, Tsujimoto K, Kikuchi K, Kurata Y, Sasa T, Umeno M, 2006. Design optimization of ADS plant proposed by JAERI. Nuclear Instruments and Methods in Physics Research A, Vol 562, pp 646–649.

Salvatores M, Slessarev I, Tchistiakov A, Ritter G, 1997. The potential of accelerator-driven systems for transmutation or power production using thorium or uranium fuel cycles. Nuclear Science and Engineering, Vol 126, pp 333–340.

Seltborg P, Jacqmin R, 2001. Spallation Neutron Source Effects in a sub-critical System. In Proc. Acc App/ADTTA'01, Reno, NV, USA.

Seltborg P, Wallenius J, Tuček K, Gudowski W, 2003. Definition and Application of Proton Source Efficiency in accelerator-driven Systems. Nuclear Science and Engineering, Vol 145, pp 390–399.

Simmons B E, King J S, 1958. A Pulsed Technique for Reactivity Determination. Nuclear Science and Engineering 3, pp 595–608.

Sjöstrand N G, 1956. Measurement on a subcritical reactor using a pulsed neutron source. Arkiv för fysik, Vol 11, No 13.

Sobolev V, Aoust, T WalleniusJ , Fokau A, Chen X, Rineiski A, 2007. Neutronic performances of EFIT-400(AFTRA) Reference Cores at the beginning of operation. Deliverable 3.2, IP EUROTRANS.

Spriggs G D, 1997. Two-Region Kinetic Model for Reflected Reactors. Annals of Nuclear Energy, Vol 24, No 3, pp 205–250.

Tsujimoto K, Sasa T, Nishihara K, Oigawa H, Takano H, 2004. Neutronics design for lead-bismuth cooled accelerator-driven system for transmutation of minor actinide. Journal of Nuclear Science and Technology, Vol 41, pp 21–36.

Tuček K, Wallenius J, Gudowski W, 2004. Coolant void worth in fast breeder reactors and accelerator-driven transuranium and minor-actinide burners. Annals of Nuclear Energy, Vol 31, pp 1783–1801.

Wallenius J, Pillon S, Zaboudko L, 2006. Fuels for accelerator-driven systems. Nuclear Instruments and Methods in Physics Research Section A, Vol 562, pp 625–629.

Yang W S, Mercatali L, Taiwo T A, Hill R N, 2001. Effects of Buffer Thickness on ATW Blanket Performances. In Proc. AccApp/ADTTA'01, Reno, NV, USA.

Zhang Y, Fokau A, Wallenius J, 2010. Safety analysis of a compact ADS with nitride fuel (to be published).

8 List of publications

Andrei Fokau, Youpeng Zhang, Shinya Ishida, Janne Wallenius, 2010. A source efficient ADS for minor actinides burning. Annals of Nuclear Energy, Vol 37, pp 540–545.

Youpeng Zhang, Janne Wallenius, 2010. Transmutation of Americium in a Medium Size Sodium Cooled Fast Reactor Design. Annals of Nuclear Energy (in press).

Calle Berglöf, 2010. Spatial and Source Multiplication Effects on the Area Ratio Reactivity Determination Method in a Strongly Heterogeneous Subcritical System. Nuclear Science and Engineering (accepted for publication).

Patricia Fernandez, 2009. Transmutation of minor actinides in a sodium cooled fast reactor. M.Sc. Thesis, Division of Reactor Physics, KTH, Stockholm.

Erdenechimeg Suvdantsetseg, 2009. Optimization of safety coefficients in BWR transmutation. M.Sc. Thesis, Division of Reactor Physics, KTH, Stockholm.

Janne Wallenius, 2009. CONFIRM: Collaboration on Nitride Fuel Irradiation and Modelling. Final report, KTH, Stockholm.

9 List of participation in conferences and project meetings

Calle Berglöf

- EUROTRANS ECATS meeting in Aix-en-Provence, France, January 27–29.
- Conference on accelerator applications (AccApp), Vienna, May 6–8.
- YALINA meeting in Madrid, Spain, May 11–17.
- Conference on Nuclear Fuel Cycle (Global-2009) in Paris, France, September 6–11.

Andrei Fokau

- Conference on Nuclear Fuel Cycle (Global-2009) in Paris, France, September 6–11.
- Material challenges for Generation IV nuclear energy systems (NOMAGE4), Studsvik, October 15–16.

Milan Tesinsky

- EUROTRANS/ECATS meeting in Aix-en-Provence, France, January 27–29.
- EUROTRANS/ECATS meeting in Mol, Belgium; October 26–28.
- Material challenges for Generation IV nuclear energy systems (NOMAGE4), Studsvik, October 15–16.

Janne Wallenius

- GETMAT meeting in Paris, January 21–22.
- ELSY meeting in Brussels, February 27.
- EUROTRANS/DEMETRA meeting in Karlsruhe, February 2–3.
- EUROTRANS/AFTRA meeting in Cadarache, February 11.
- EUROTRANS WP1.5 meeting in Lyon, March 17–18.
- EUROTRANS/DESIGN meeting in Madrid, March 26–27.
- Fe-Cr workshop in Genoa, March 30–31.
- EUROTRANS Governing Council meeting in Paris, April 2–3.
- PhD evaluation committee at EPFL, Lausanne, May 28.
- Klimat- och energipolitik, Tylösand, August 26.
- Estonian nuclear masters programme meeting, Tallinn, September 4.
- Conference on Nuclear Fuel Cycle (Global-2009) in Paris, France, September 6–10.
- Chernobyl field trip, September 8–9.
- EUROTRANS/DEMETRA meeting in Bologna, September 15–16.
- EUROTRANS WP1.5 meeting in Brussles, Germany, September 30 – October 1st.
- EUROTRANS/DESIGN CC meeting in Brussels, October 1–2.
- Material challenges for Generation IV nuclear energy systems (NOMAGE4), Studsvik October 15–16.
- Fe-Cr workshop in Madrid, November 2.
- SUCCESS proposal preparation meeting, Karlsruhe, November 4–5.
- ESS workshop in Lund, December 2.
- CEFOS workshop on nuclear waste management, Göteborg, December 15–17.

Youpeng Zhang

- Material challenges for Generation IV nuclear energy systems (NOMAGE4), Studsvik, October 15–16.